Extracellular microRNAs in human circulation are associated with miRISC complexes that are accessible to anti-AGO2 antibody and can bind target mimic oligonucleotides

Hirosha Geekiyanage[a], Shima Rayatpisheh[b], James A. Wohlschlegel[b], Robert Brown Jr[c], and Victor Ambros[a,1]

[a]Department of Molecular Medicine, University of Massachusetts Medical School, Worcester, MA 01605; [b]Department of Biological Chemistry, Geffen School of Medicine, University of California, Los Angeles, CA 90095; and [c]Department of Neurology, University of Massachusetts Medical School, Worcester, MA 01605

Edited by Iva Greenwald, Columbia University, New York, NY, and approved August 12, 2020 (received for review April 28, 2020)

MicroRNAs (miRNAs) function cell-intrinsically to regulate gene expression by base-pairing to complementary mRNA targets while in association with Argonaute, the effector protein of the miRNA-mediated silencing complex (miRISC). A relatively dilute population of miRNAs can be found extracellularly in body fluids such as human blood plasma and cerebrospinal fluid (CSF). The remarkable stability of circulating miRNAs in such harsh extracellular environments can be attributed to their association with protective macromolecular complexes, including extracellular vesicles (EVs), proteins such as Argonaut 2 (AGO2), or high-density lipoproteins. The precise origins and the potential biological significance of various forms of miRNA-containing extracellular complexes are poorly understood. It is also not known whether extracellular miRNAs in their native state may retain the capacity for miRISC-mediated target RNA binding. To explore the potential functionality of circulating extracellular miRNAs, we comprehensively investigated the association between circulating miRNAs and the miRISC Argonaute AGO2. Using AGO2 immunoprecipitation (IP) followed by small-RNA sequencing, we find that miRNAs in circulation are primarily associated with antibody-accessible miRISC/AGO2 complexes. Moreover, we show that circulating miRNAs can base-pair with a target mimic in a seed-based manner, and that the target-bound AGO2 can be recovered from blood plasma in an ∼1:1 ratio with the respective miRNA. Our findings suggest that miRNAs in circulation are largely contained in functional miRISC/AGO2 complexes under normal physiological conditions. However, we find that, in human CSF, the assortment of certain extracellular miRNAs into free miRISC/AGO2 complexes can be affected by pathological conditions such as amyotrophic lateral sclerosis.

Argonaut | extracellular microRNA | human plasma | cerebrospinal fluid | AGO2

MicroRNAs (miRNAs) are endogenous small RNAs of 21 to 22 nucleotides that regulate gene expression by base-pairing to mRNA targets and causing their translation repression and/or degradation (1–3). Depending on the cell type, there can be ∼10,000 to 120,000 miRNA molecules per cell (4). Although miRNAs function cell-intrinsically, extracellular miRNAs can be found in tissue culture medium (5) or circulating in body fluids, such as human blood plasma (6, 7) and cerebrospinal fluid (CSF) (8). Many of the miRNAs detected in circulation are known to be expressed tissue-specifically, and profiles of circulating miRNAs can change depending on physiological or pathological conditions (9, 10). Therefore, circulating miRNAs can reflect the status of internal tissues and organs, and hence can serve as diagnostic biomarkers for diseases, including cancer (11, 12), neurological disease (10, 13), and liver toxicity (14).

The remarkable stability of miRNAs in cell-free body fluids can be attributed to their reported association with various macromolecular complexes, including membranous extracellular vehicles (EVs) (15), high-density lipoproteins (16), or the miRNA-mediated silencing complex (miRISC) effector protein Argonaute 2 (AGO2) (5–7). Reports vary on the distribution of circulating miRNAs among such distinct carrier complexes. Numerous reports show that miRNAs can be readily extracted from fractions of blood plasma or extracellular culture medium enriched for EVs (11, 17–19). In contrast, extracellular miRNAs have been found associated with apparent ribonucleoprotein (RNP) complexes that are appreciably smaller than EVs. Size-exclusion chromatography of human plasma demonstrated that miRNA-associated AGO2 complexes were enriched in fractions corresponding to the approximate size of Argonaute, and not in the fractions corresponding to 100-nm-diameter vesicles (6). In a qRT-PCR profiling of 375 miRNAs in these size-exclusion chromatography fractions of human plasma, greater than 67% of the assayed miRNAs were associated with fractions containing AGO2 protein, and a corresponding portion of plasma miRNAs could be recovered by AGO2 immunoprecipitation from plasma (6). Similarly, other studies have indicated that a significant

Significance

MicroRNAs (miRNAs) are abundant inside cells, where they regulate gene expression posttranscriptionally, but are also found in circulation as remarkably stable extracellular constituents of body fluids such as human blood plasma and cerebrospinal fluid. We observed that these circulating miRNAs are predominantly associated with free Argonaut 2 (AGO2) complexes that are accessible to immunoprecipitation by AGO2 antibodies and are able to base-pair with complementary target RNAs, suggesting that, under normal physiological conditions, circulating miRNAs are largely contained in functional miRNA-mediated silencing complexes (miRISCs). However, we observe that, under certain pathological conditions, more miRNAs become associated with complexes other than free AGO2/miRISC, suggesting that the assortment of circulating miRNAs into distinct complexes offers a potential new dimension to miRNA-based diagnostics.

Author contributions: H.G., S.R., J.A.W., R.B., and V.A. designed research; H.G. and S.R. performed research; H.G., S.R., J.A.W., R.B., and V.A. analyzed data; and H.G. and V.A. wrote the paper.

The authors declare no competing interest.

This article is a PNAS Direct Submission.

[1]To whom correspondence may be addressed. Email: victor.ambros@umassmed.edu.

This article contains supporting information online at https://www.pnas.org/lookup/suppl/doi:10.1073/pnas.2008323117/-/DCSupplemental.

First published September 14, 2020.

portion of miRNAs in blood plasma and/or cell culture media could be separated from EVs by ultracentrifugation (7) and fractionated together with AGO2 in subsequent ultrafiltration (5, 20). It is possible that the yield of miRNAs recovered from EVs could depend on whether the particular protocol used to enrich for EVs can effectively distinguish between miRNAs encapsulated within EVs or, alternatively, miRNAs associated with the exterior surface of the EVs (Fig. 1).

The underlying mechanisms by which cells export miRNAs are poorly understood, and it is not known which extracellular carrier complexes, such as EVs or free AGO2, may reflect active versus passive export of miRNAs from cells. In some disease contexts (14, 21, 22), cells can release miRNAs passively due to injury, chronic inflammation, apoptosis, or necrosis. There is also evidence that cells can actively export miRNAs by selectively packaging them into particular carriers (23–27), perhaps to maintain cell homeostasis or send signals to recipient cells. For example, certain cancer cell lines appear to selectively export let-7 family miRNAs into the extracellular milieu via EVs, conceivably to maintain their oncogenic state (28). Similarly, miR-126 released into apoptotic bodies by cells during atherosclerosis is reported to communicate paracrine alarm signals to vascular cells, which in turn produce protective chemokines (24).

The apparent stability of miRNAs in circulation supports the hypothesis that extracellular miRNAs could reflect a mode of RNA-mediated intercellular communication, such that miRNAs produced in one cell could function to regulate gene expression in another cell. In this regard, there is evidence that miRNAs in circulation could be functional in recipient cells, either in cell culture or in the intact mouse (15, 29–32). However, the concentration of extracellular miRNAs in blood plasma is in the order of ~5 pM (33), far less than the concentrations considered to be minimal for intracellular function, which are estimated to be at least ~26 pM (34), or even in the nanomolar range when considering intratarget pool competition in the cytoplasm (4). Therefore, the sparse concentration of miRNAs in circulation would need to be dramatically concentrated upon uptake in order to function in a recipient cell. However, it is possible that the miRNAs detected in circulation may correspond to a diluted sample of more concentrated (and thus potentially functional) populations of extracellular miRNAs in the interstitial milieu of tissues.

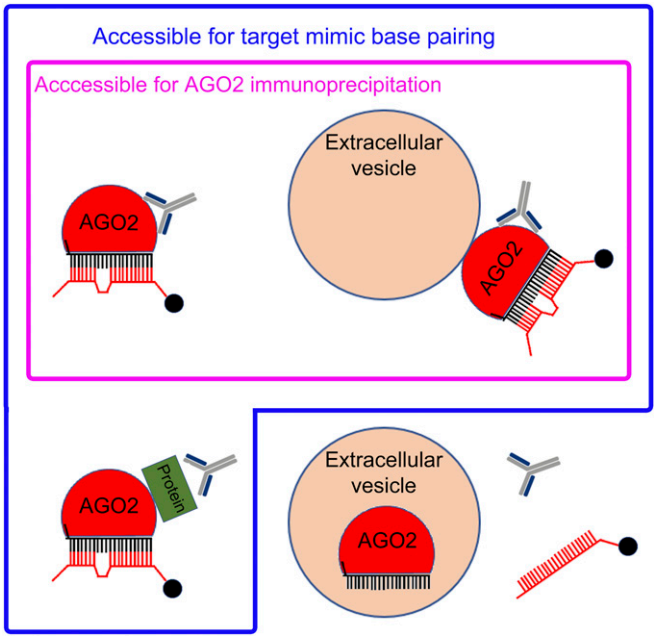

Fig. 1. Model of circulating miRNA association with carrier complexes. A portion of circulating miRNAs are proposed to be associated with free miRISC/AGO2 complexes that are accessible for base pairing to target mimic oligonucleotides (blue enclosure), a subset of which are accessible for binding to anti-AGO2 antibodies (pink enclosure).

In this study, we comprehensively characterized the profiles of circulating miRNAs associated with AGO2 in human plasma and CSF by immunoprecipitating AGO2 under native conditions, followed by small RNA sequencing. Our studies show that a major fraction of miRNAs in circulation are primarily associated with AGO2 complexes that readily bind to anti-AGO2 antibodies under native conditions, and therefore are not enclosed within vesicles. We also find that a subfraction of the population of certain circulating miRNAs are inaccessible for AGO2 immunoprecipitation and therefore apparently are associated with other complexes, such as other Argonaute proteins or the interiors of extracellular vesicles. We find that, for particular miRNAs in CSF samples, the AGO2 association profiles can differ significantly under pathological conditions such as elevated intracranial pressure (ICP) or amyotrophic lateral sclerosis (ALS) compared with healthy CSF samples, suggesting that AGO2 immunoprecipitation can potentially enhance the resolution of miRNA biomarker screening.

We assessed the target binding potential of miRISC in circulation by introducing an affinity matrix-linked target mimic into human plasma samples under native conditions and subsequently assessing depletion and recovery of the complementary miRNA via quantitative real-time PCR (qRT-PCR) and small-RNA sequencing. By using complementary target RNA against two distinct miRNAs, we show that the miRNAs associated with free miRISC/AGO2 in circulation can base-pair with their RNA targets in a seed-guided manner, and therefore could potentially function in the event that they were to be taken up by cells in sufficient quantities.

Results

miRNAs Can Be Depleted and Recovered from Human Blood Plasma by Native Immunoprecipitation with Anti-AGO2 Antibody. In order to identify plasma miRNAs associated with free, antibody-accessible AGO2, we immunoprecipitated AGO2 from 200 μL of human blood plasma samples using 10 μg of anti-AGO2 antibody with overnight incubation (Fig. 2*A*, *SI Appendix*, Fig. S1, and *Materials and Methods*). Anti-AGO2 Western blot analysis showed a band at ~97 kDa, which is the expected molecular weight of AGO2, in the AGO2 immunoprecipitation, while there was no such band evident for control IgG immunoprecipitation (Fig. 2*B*).

To confirm that the 97-kDa band reacting with anti-AGO2 in our Western blots was indeed immunoprecipitated AGO2 and not cross-reacting protein(s), we conducted mass spectrometry analysis of gel sections cut at specific ranges of molecular weights (Fig. 2*C*). Mass spectrometry analysis confirmed the presence of AGO2 protein in AGO2 immunoprecipitation at the correct molecular weight section (slice C, 75 to 100 kDa) and the absence of AGO2 in the control IgG immunoprecipitation. AGO2 protein was only detected in the gel slice corresponding to ~75 to 100 kDa and not at any other molecular weight (Fig. 2*D* and Dataset S1).

qRT-PCR analysis showed that miR-16 was depleted from plasma by AGO2 immunoprecipitation compared with control IgG immunoprecipitation and that the depleted miR-16 could be recovered from the immunoprecipitated beads (Fig. 2*E*). This indicates that miR-16 in human blood plasma is largely associated with antibody-accessible AGO2. To comprehensively identify the miRNAs associated with these complexes, we conducted small-RNA sequencing of RNA remaining in the supernatant after AGO2 immunoprecipitation and RNA recovered from the AGO2-immunoprecipitated beads. Quantitative analysis of RNA-seq data was conducted by normalizing the UMI counts of the circulating miRNA across the samples to a standard quantity of spike-in miRNA (cel-miR-39) that was added to each sample

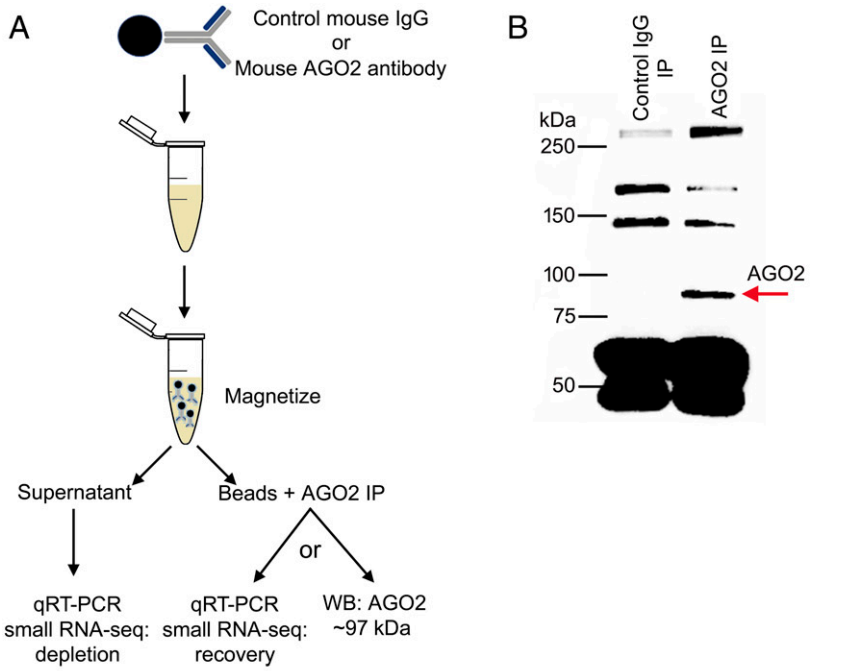

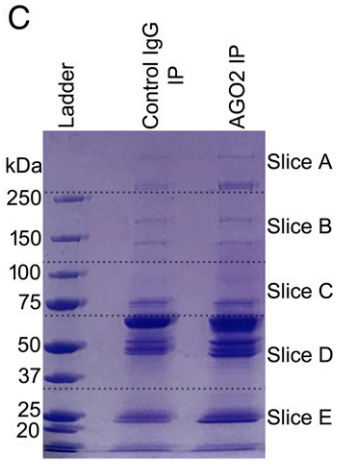

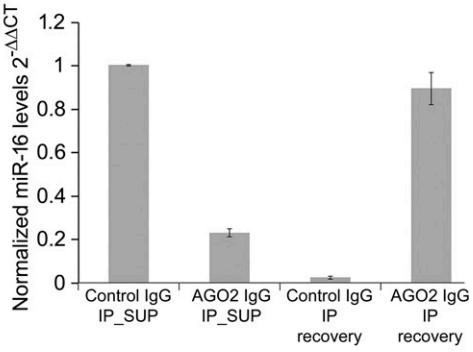

D

	Control IgG immunoprecipitaion					AGO2 immunoprecipitaion				
	Slice A	Slice B	Slice C	Slice D	Slice E	Slice A	Slice B	Slice C	Slice D	Slice E
AGO2 (peptide spectral counts)	0	0	0	0	0	0	0	38	0	0

Fig. 2. Immunoprecipitation of circulating miRNA from human blood plasma. (*A*) Schematic showing the immunoprecipitation (IP) protocol where bead-conjugated mouse AGO2 antibodies are incubated overnight at 4 °C in blood plasma under native conditions (absence of detergent or any other additive). The beads are removed by magnetizing, and RNA extracted from the supernatant is subjected to qRT-PCR and/or small-RNA sequencing to detect the miRNAs depleted by AGO2 immunoprecipitation. The magnetized beads are processed either for RNA extraction followed by qRT-PCR and/or small-RNA sequencing to assess miRNA recovery, or for protein extraction and subsequent Western blotting using a rabbit anti-AGO2 antibody (orthogonal to the immunoprecipitation antibody). (*B*) Western blot probed with anti-AGO2 antibody to assess AGO2 associated with the captured beads following AGO2 immunoprecipitation. The red arrow shows that an AGO2 band at ~97 kDa is detected in the anti-AGO2 immunoprecipitate but absent from the control IgG immunoprecipitate. (*C*) Coomassie staining following SDS/PAGE shows the sections that were sliced according to ranges of molecular weight and subjected to mass spectrometry (Dataset S1). (*D*) Summary of AGO2 peptide spectral counts as determined by tandem mass spectrometry. AGO2 was only detected in slice C (75 to 100 kDa) in immunoprecipitation using anti-AGO2. (*E*) qRT-PCR analysis of miR-16 levels in the plasma supernatant and beads to display depletion and recovery following immunoprecipitation of control IgG and AGO2. Relative miRNA levels are normalized to the mean miRNA levels of control IgG supernatant samples following normalization of all samples to the cel-miR-39 spike-in. Error bars represent SE of mean (SEM) derived from three or more experiments. Statistical significances were determined by Student *t* tests ($P \leq 0.05$).

at the Trizol extraction step, thus allowing a direct measurement of depletion and recovery (*Materials and Methods*). We observed that essentially all of the miRNAs detected by RNA sequencing were at least partially depleted from plasma by AGO2 immunoprecipitation compared with control IgG immunoprecipitation (Fig. 3*A*), suggesting that many plasma miRNAs are associated with antibody-accessible AGO2. Many of the depleted miRNAs seem to be efficiently recovered from the anti-AGO2 beads, with some exceptions,

especially among the less abundant miRNAs (Fig. 3*B*). Across all miRNAs detectable in human blood plasma samples ($n = 2$) by our small RNA sequencing, we observed an average depletion of 78% (Fig. 3*C*). We identified 304 miRNAs that were depleted at least 50% by anti-AGO2 immunoprecipitation and 19 miRNAs that were less than 50% depleted by AGO2 immunoprecipitation (Fig. 3*C*). Of the 130 miRNAs that we detected by small RNA sequencing in 5 biological replicates, 114 were depleted more than 50% in a statistically significant manner ($P \leq 0.05$), while 11 miRNAs were depleted less than 50% in a statistically significant manner, and the remaining 5 miRNAs showed an average depletion of less than 50% but did not meet statistical significance (*SI Appendix*, Fig. S2, and Dataset S2).

These depletion and recovery data suggest that most circulating miRNAs in our human plasma samples are predominantly associated with AGO2 complexes that are free to interact with anti-AGO2 antibodies under the conditions of our immunoprecipitation experiments. The poorly immunoprecipitated miRNAs could be associated with AGO2 complexes that have their anti-AGO2 binding epitopes masked by other proteins, or they could be associated with other RNA-binding proteins, such as AGO1/3/4, or they could be enclosed within vesicles (Fig. 1). It should be noted that our immunoprecipitation experiments are conducted using essentially native plasma, and, in particular, the immunoprecipitation conditions do not include any detergent and hence should maintain any extracellular membranous vesicles in their intact state.

Most of the miRNAs in Normal Human CSF Can Be Depleted by AGO2 Immunoprecipitation. We conducted AGO2 immunoprecipitation using 250 μL of human CSF samples from a cohort of healthy individuals ($n = 3$) and assessed miRNA depletion using small RNA sequencing (Fig. 4*A*). For the 203 miRNAs represented in our sequencing data, the average depletion was 62% (Fig. 4*D*). Out of the 155 miRNAs that were at least 50% depleted from CSF by anti-AGO2 antibodies, 126 miRNAs showed statistical significance, and, out of the 48 miRNAs that exhibited less than 50% depletion, 22 miRNAs showed statistical significance (Dataset S3). This suggested that the majority of the miRNAs in CSF samples from healthy individuals are associated with antibody-accessible AGO2 complexes.

The results reported above, showing immunoprecipitation of miRNAs from plasma and CSF using anti-AGO2 antibodies, suggest that a major portion of circulating miRNAs in blood plasma and CSF are associated with AGO2 that is accessible to bind anti-AGO2 antibody. However, mere recovery of miRNA from anti-AGO2 IP does not in itself confirm that the miRNAs are loaded into Argonaute in the standard manner, or even directly associated with Argonaute. If the miRNAs are loaded into AGO2, then there are two predictions: (*i*) circulating miRNAs should exhibit the capacity to bind to a target via seed-mediated base pairing and (*ii*) miRNAs and their AGO2 partner proteins should be present in an ∼1:1 ratio in plasma or CSF. In the following two sections, we test these predictions.

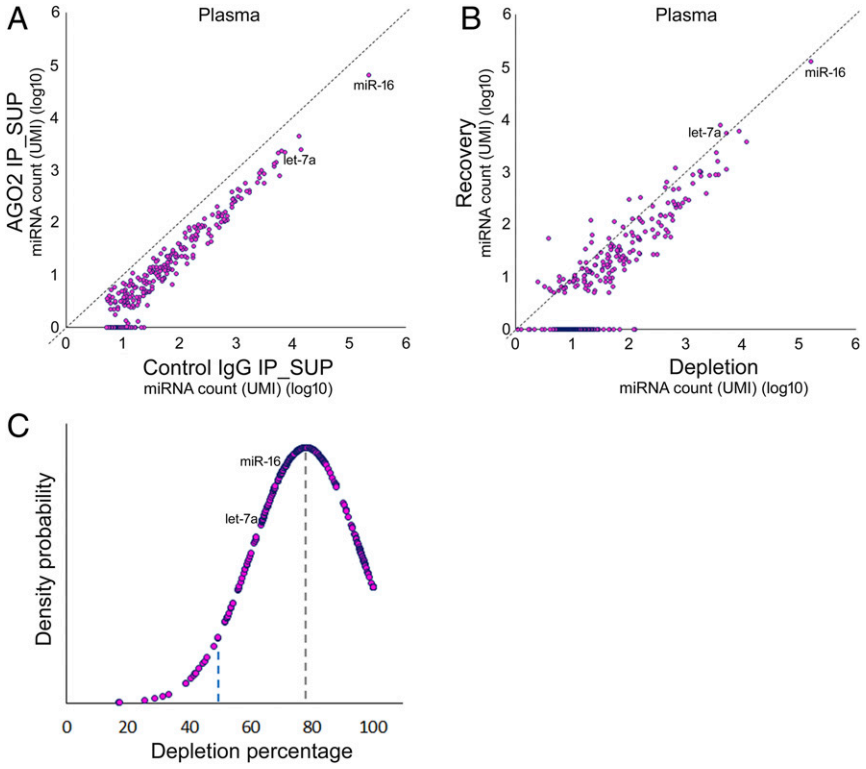

Fig. 3. Plasma miRNAs can be depleted by AGO2 immunoprecipitation. (*A*) Small-RNA sequencing of RNAs extracted from plasma supernatant following control IgG (*x*-axis; $n = 2$) and AGO2 (*y*-axis; $n = 2$) immunoprecipitation. A cel-miR-39 spike-in was included to normalize the data to the original sample volume, allowing a direct comparison of the yields of miRNAs from control and experimental samples. Essentially all of the miRNAs detected in the sequencing dataset are below the diagonal line, indicating a general depletion of miRNAs from plasma by AGO2 immunoprecipitation. (*B*) Small RNA sequencing analysis of depletion vs. recovery in plasma. Depletion was calculated by subtracting AGO2 immunoprecipitated supernatant miRNA counts from control IgG immunoprecipitated supernatant miRNA counts, and recovery was calculated by subtracting control IgG-immunoprecipitated miRNA counts from the AGO2-immunoprecipitated miRNA counts. (*C*) Distribution of the percent depletions by anti-AGO2 immunoprecipitation for 323 miRNAs ($n = 2$ samples). Average depletion was ∼78% (gray dashed line); 19 of the 323 miRNAs were depleted less than 50% (blue dashed line). The positions of miR-16 and let-7a are labeled.

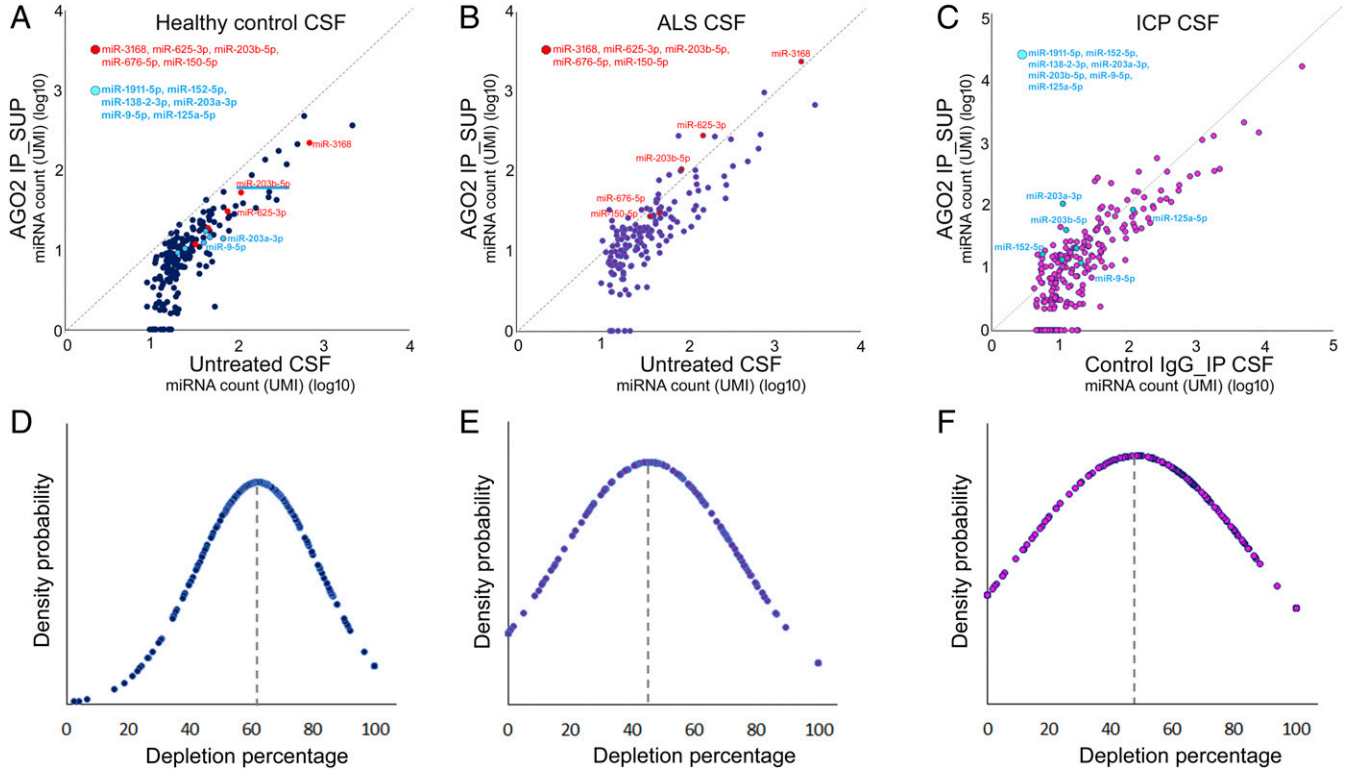

Fig. 4. The profiles of miRNAs depleted by AGO2 immunoprecipitation from healthy CSF samples and CSF from patients with ALS or ICP. (*A*) Small-RNA sequencing of supernatant following control IgG (*x*-axis; $n = 3$) and AGO2 (*y*-axis; $n = 3$) immunoprecipitation in CSF from healthy individuals. Almost all miRNAs are below the diagonal line, indicating a general depletion of almost all miRNAs in CSF from healthy individuals. (*B*) Small-RNA sequencing of supernatant following control IgG (*x*-axis; $n = 3$) and AGO2 (*y*-axis; $n = 3$) immunoprecipitation in CSF from ALS patients. Fewer miRNAs (than in *A*) are below the diagonal line for the ALS samples, indicating an increase in miRNAs refractory to immunoprecipitation in the CSF from ALS patients compared with healthy individuals. (*C*) Small-RNA sequencing of supernatant following control IgG (*x*-axis; $n = 2$) and AGO2 (*y*-axis; $n = 2$) immunoprecipitation in CSF from patients with ICP. Again, fewer miRNAs (than in *A*) are below the diagonal line for the ICP samples, indicating an increase in miRNAs refractory to immunoprecipitation in the CSF from ICP patients compared with healthy individuals. For *A*–*C*, the red dots represent the miRNAs that are refractory to depletion ($P \leq 0.05$) in ALS CSF (*B*) but are efficiently depleted from control CSF ($P \leq 0.05$ or $P \leq 0.1$; *A*); the turquoise dots represent the miRNAs that are efficiently depleted ($P \leq 0.05$) in healthy control CSF (*A*) but refractory to depletion ($P \leq 0.05$) by AGO2 immunoprecipitation in CSF from ICP patients (*C*). miR-203b-5p is refractory to depletion in both ALS and ICP CSF samples compared with CSF samples from healthy individuals, and thus represented in an underlined (turquoise) red dot in *A*. (*D*–*F*) Distribution of miRNA depletion by AGO2 immunoprecipitation in healthy control CSF (*D*), ALS CSF (*E*), and ICP CSF (*F*). The average depletions (dashed gray lines) are ∼62%, ∼45%, and 48%, respectively. The UMI count for each sample is normalized to the spike-in cel-miR-39.

Circulating miRNAs Can Base-Pair Sequence-Specifically to a Target Mimic Oligonucleotide. In order to assess whether AGO2-associated plasma miRNAs are accessible for base-pairing with a target, we incubated 5 pmol of biotinylated 2′-O-methyl RNA oligonucleotides (conjugated to streptavidin beads) that were fully complementary to either miR-16 or let-7a in plasma for 15 min at room temperature (Fig. 5 *A* and *B*, *SI Appendix*, Fig. S3, and *Materials and Methods*).

qRT-PCR data showed that a target oligonucleotide complementary to miR-16 depleted ∼90% of miR-16 from plasma, whereas let-7a was not depleted by the miR-16 target oligo (Fig. 5*C*). Conversely, using a target oligo complementary to let-7a, we observed depletion (∼50% via qRT-PCR) of let-7a from plasma and essentially no depletion of miR-16 (Fig. 5*C*). These results indicate that the miR-16 and let-7a complementary targets specifically depleted their cognate miRNAs from human blood plasma. Consistent with sequence-specific capture, miR-16 (but not let-7a) was recovered from miR-16 target oligonucleotide-conjugated beads (Fig. 5*D* and *SI Appendix*, Fig. S4; recovery protocol described in *Materials and Methods*).

If the miR-16 target oligonucleotides were capturing miR-16 miRISC through Argonaute-facilitated (seed sequence-mediated) base pairing, then we expect that the miR-16 target should also deplete other members of the miR-16 seed family from plasma. We conducted qRT-PCR assays on RNA from plasma incubated with miR-16 target oligonucleotide or scrambled oligo to measure the specific depletion of a selected set of miRNAs, including the miR-16 family members miR-16, miR-15a, and miR-195 and other non–miR-16 family miRNAs, miR-451, miR-92, miR-223, miR-1249, miR-22, miR-126, miR-142-3p, miR-4454, and miR-191. We observed that the target oligonucleotides complementary to miR-16 depleted the miR-16 family, but did not appreciably deplete the non–miR-16 family miRNAs tested, with the exception of miR-191 (*SI Appendix*, Fig. S5; see additional discussion below regarding this partial depletion of miR-191 by miR-16 target oligo).

In order to comprehensively evaluate the sequence specificity of binding of circulating miRNAs with a defined target sequence, we conducted small RNA sequencing from the plasma supernatant (to assess depletion) and the bead-bound miRNAs (to assess recovery) after incubation of the beads containing the miR-16 target oligo. Small RNA sequencing analysis showed statistically significant depletion of miR-16 and the miR-16 seed family members miR-15a, miR-15b, and miR-195. Interestingly, we also observed depletion of members of another seed family of miRNAs, miR-103 and miR-107 (Fig. 6 *A* and *B*). Depletion of the miR-103/107 family can be accounted for by the fact that the miR-103/107 seed (GCAGCAU) is similar enough to the miR-16 seed (AGCAGCA) such that miR-16 target oligonucleotide contains a nucleotide 2–7 hexamer seed match to miR-103/107

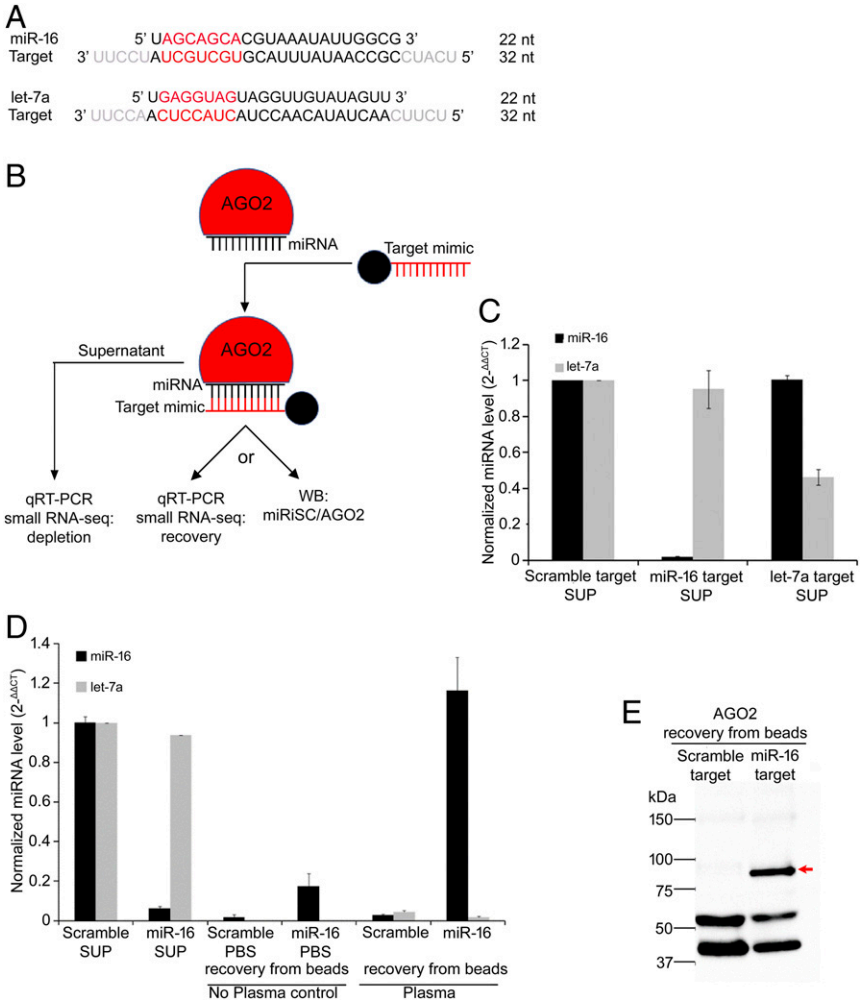

Fig. 5. Target mimic oligonucleotides can base-pair with plasma miRNAs, capturing the cognate miRNA, along with AGO2. (*A*) Sequence complementarity of miR-16 and let-7a target mimic oligonucleotides to their cognate miRNAs. There are five extra nucleotide overhangs on the 5′ and 3′ ends of each of the target mimic oligonucleotides. (*B*) Schematic showing the affinity matrix-linked target mimic assay where the biotinylated target mimic is conjugated to streptavidin beads and incubated with native plasma, without detergent or additives, for 15 min at room temperature. The beads were removed by magnetizing, and the supernatant and the magnetized beads were processed for RNA extraction or protein gel electrophoresis and Western blotting using anti-AGO2 antibody. (*C*) qRT-PCR analysis of the plasma supernatant following the incubation with a target mimic oligo against miR-16 or let-7a. miR-16 was depleted from plasma with a target oligo against miR-16, whereas let-7a was not depleted.. Let-7a was depleted from plasma with a target oligo against let-7a, while miR-16 was not depleted. (*D*) qRT-PCR analysis of the recovery of plasma miR-16 following incubation with a target mimic fully complementary to miR-16 or a scrambled target mimic. *Materials and Methods* and *SI Appendix*, Fig. S4, describe the protocol for recovering miRNAs from the target mimic capture beads. "No plasma control" represents incubation of bead-conjugated target mimics in PBS. Relative expression levels shown are normalized to the spike-in cel-miR-39 and to the scrambled target mimic-incubated plasma supernatant. Error bars represent SE of mean (SEM) derived from three or more experiments. Statistical significances were determined by Student *t* tests. (*E*) Western blot probed with anti-AGO2 antibody to assess the AGO recovered from the miR-16 and scrambled target mimic-conjugated beads following incubation in plasma. The red arrow shows the AGO2-specific band at ~97 kDa present in the sample from the miR-16 target oligo beads and absent from the scrambled oligo beads.

(*SI Appendix*, Fig. S6). Similar to the qRT-PCR data reported above, our small RNA sequencing data also indicated a partial depletion (albeit not statistically significant by Deseq2 analysis) of miR-191 with the target oligo complementary to miR-16 (*SI Appendix*, Fig. S6*J*). We note that miR-191 has partial complementarity in its seed region and 3′ supplementary region to the miR-16 target/capture oligo, which perhaps could account for the partial depletion of miR-191 by this miR-16 target oligonucleotide. Only the recovery (from beads) of miR-16 was statistically significant (Deseq2 analysis) compared to the incubation of a scrambled oligo (*SI Appendix*, Fig. S6 *A* and *B*) that did not have a specific target. We were unable to recover all of the miR-16 that was depleted, perhaps due to degradation during the lengthy recovery protocol that includes a high-temperature incubation (*SI Appendix*, Fig. S6).

Similarly, small RNA sequencing showed that let-7a and its family members, let-7b, let-7c, and let-7d, were depleted from plasma when a target fully complementary to let-7a was used (Fig. 6 *C* and *D*). let-7b, let-7c, and let-7d differ in sequence from let-7a in their nonseed sequences, indicating that the target oligonucleotide captures these miRNAs by seed-mediated base-pairing, characteristic to miRISC target recognition (*SI Appendix*, Fig. S7). qPCR assays indicated that let-7a was ~50% depleted from plasma by the let-7a complementary target mimic oligonucleotide (Fig. 5*C*). However, small-RNA sequencing data showed that let-7a was ~80% depleted by the same let-7a target mimic (*SI Appendix*, Fig. S7*A*). This apparent discrepancy between qPCR and small RNA sequencing could reflect a relaxed specificity of the qRT-PCR assay for let-7a, such that other (relatively less depleted) let-7 family members may have been

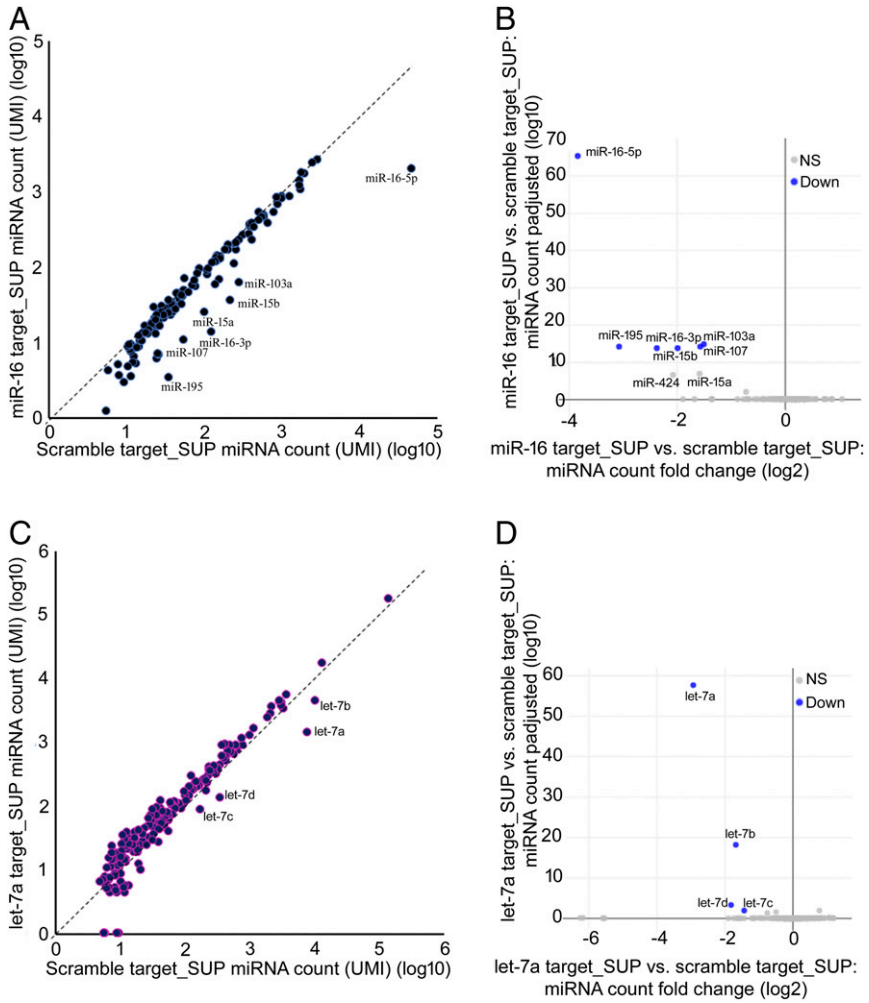

Fig. 6. Target mimic oligonucleotides specifically deplete their complementary miRNAs. (*A* and *B*) Small-RNA sequencing of plasma supernatant following incubation with scrambled oligonucleotide (x-axis) or miR-16 ($n = 3$; *A*) or let-7a ($n = 2$; *B*) target mimic (*y*-axis). (*C* and *D*) Deseq2 statistical analysis conducted with FDR threshold at 5% (adjusted *P* value ≤ 0.05) and fold change set to >2 shows the miRNAs that are depleted in a statistically significant manner by miR-16 target mimic (*C*) or let-7a target mimic (*D*). The UMI counts are normalized to the spike-in cel-miR-39.

detected in addition to let-7a. In this respect, we note that, in our small RNA sequencing data, the cumulative average depletion of let-7 family members (let-7a, let-7b, let-7c, let-d, let-7e, let-7f, let-7g, and let-7i) was ∼34% (*SI Appendix*, Fig. S7*F*).

These results using affinity matrix-linked target mimics against miR-16 and let-7a show that circulating miR-16 and let-7 retain the capacity to engage in sequence-specific target binding in a manner consistent with their association with active miRISC.

Stoichiometry of miRNA and Argonaute in Circulating miRISC/AGO2 Complexes. We quantified the amount of AGO2 immunoprecipitated from human plasma by anti-AGO2 antibodies using Western blotting and a purified human AGO2 protein as a quantification standard. The results indicate a concentration of antibody-accessible AGO2 in plasma of ∼35 pM (*SI Appendix*, Fig. S8). Similarly, we measured the amount of antibody-accessible AGO2 in CSF to be ∼100-fold less than that in plasma (*SI Appendix*, Fig. S9 *A* and *B*). This corresponds roughly to the relative levels of certain major miRNAs in CSF compared with plasma. For example, miR-16 was estimated to be ∼640 fM in plasma and ∼1.6 fM in CSF (*SI Appendix*, Fig. S9 *C* and *D*); miR-451 was estimated to be ∼2.6 pM in plasma and ∼15 fM in CSF (*SI Appendix*, Fig. S9 *E* and *F*).

We then quantified the amount of AGO2 recovered by oligonucleotides complementary to miR-16 or miR-451 (*SI Appendix*, Fig. S10). We determined that the amount of AGO2 recovered from 200 μL of plasma by each miRNA target oligonucleotide was similar to the amount of the respective miRNA in the same volume of plasma. miR-16 levels in plasma were determined to be about 640 fM (*SI Appendix*, Fig. S9*C*), which corresponds to ∼0.13 fmoles in 200 μL; the amount of miR-16–bound AGO2 recovered from 200 μL of plasma was similarly ∼0.1 fmoles (*SI Appendix*, Fig. S10 *A* and *B*). Likewise, miR-451 levels in plasma were determined to be an average of ∼2.6 pM (*SI Appendix*, Fig. S9*E*), which corresponds to ∼0.5 fmoles per 200 μL; the amount of miR-451–bound AGO2 recovered from 200 μL of plasma was determined to be ∼0.56 fmoles (*SI Appendix*, Fig. S10 *C* and *D*). The essentially 1:1 ratio between the respective circulating miRNA and the AGO2 recovered by miRNA-specific target mimic supports the conclusion that circulating miR-16 and miR-451 are associated with bona fide miRISC.

Stability of Circulating miRISC Complexes against Sample Freeze/Thaw Cycles and during Incubations for Immunoprecipitation and Target Oligo Capture. Generally, our fresh plasma and CSF samples were aliquoted and frozen at −80 °C and thawed at the time

of the experiments. Therefore, it was a formal possibility that some of the properties of circulating miRISC that we observed, such as their accessibility to immunoprecipitation by anti-AGO2 antibodies and base-pairing with target oligonucleotides, could be a consequence of their release from the protection of hypothetical higher-order complexes by a single cycle of freezing and thawing.

Accordingly, fresh (never frozen) plasma samples were collected from volunteers, split into aliquots, and, for each sample, one never-frozen aliquot was kept in ice (4 °C) for (immediate) further analysis while another aliquot was subjected to one cycle of freezing (−80 °C). Both the freeze-thawed aliquots and the fresh (never-frozen) aliquots were processed in parallel for AGO2 immunoprecipitation or target mimic oligo pull-down and subsequent small RNA extraction.

We observed very similar patterns of miRNA depletion by AGO2 immunoprecipitation from frozen vs. fresh aliquots of plasma, where essentially none of the miRNAs showed statistical significance (Deseq2) in depletion between fresh vs. frozen samples (*SI Appendix*, Fig. S11)

Likewise, we used a 2′-O-methyl oligonucleotide target mimic to pull down miR-16 from frozen and fresh aliquots of otherwise identical plasma samples and observed that the miR-16 family and the miR-107/103 family miRNAs were depleted (Deseq2) similarly from plasma for both the fresh and the frozen samples (*SI Appendix*, Fig. S12).

To evaluate whether the stability of circulating miRNAs detectable in plasma can be appreciably affected by freeze-thawing or by the incubation conditions associated with our immunoprecipitation and target mimic pull-down experiments, we compared the abundance of miRNAs via small RNA sequencing between otherwise identical aliquots of fresh plasma samples (never frozen; maintained on ice) that were either processed immediately for RNA extraction ("Fresh" in *SI Appendix*, Fig. S13) and frozen (−80 °C) and thawed (*SI Appendix*, Fig. S13 *A* and *B*) or never-frozen plasma samples left at room temperature (~22 °C) for 30 min (which corresponds to the target mimic pull-down conditions; *SI Appendix*, Fig. S13 *C* and *D*) or never-frozen plasma samples left overnight at 4 °C (which corresponds to the immunoprecipitation conditions; *SI Appendix*, Fig. S13 *E* and *F*). In none of these comparisons did we detect appreciable changes (Deseq2 analysis) in miRNA profiles; the only noted exception was that miR-145-3p levels were decreased during the 30-min room temperature incubation.

These findings indicate that abundances of miRNAs in our plasma samples, and the accessibility of miRNA::carrier complexes to immunoprecipitation by anti-AGO2 or target mimic pull-down, is not an artifact of using frozen samples, nor are there appreciable changes in miRNA abundance over the course of our experimental incubations (*SI Appendix*, Figs. S11–S13).

miRNA Depletion by AGO2 Immunoprecipitation of CSF from Normal Controls Compared to Patients with CNS Pathologies. We conduced AGO2 immunoprecipitation using CSF samples from amyotrophic lateral sclerosis (ALS) patients and observed a pattern of miRNA depletion that differed from that observed in healthy CSF samples. Fewer miRNAs were efficiently depleted from ALS CSF compared with CSF from healthy individuals (Fig. 4 *A*–*D*). Overall, most miRNAs detected in normal CSF were depleted to varying levels by AGO2 immunoprecipitation (average depletion of ~62%; $n = 3$), while certain miRNAs in ALS CSF appear to be resistant to depletion by AGO2 immunoprecipitation (average depletion of ~45%; $n = 3$). For example, miR-203b-5p, miR-150-5p, and miR-676 were ~54% ($P = 0.02$), ~64% ($P = 0.01$), and ~59% ($P = 0.0003$) depleted, respectively, in healthy control CSF by AGO2 immunoprecipitation, while miR-203b-5p was not depleted at all (0%; $P = 5.0E-324$) and miR-150-5p and miR-676 were only ~31% ($P = 0.03$) and ~36% ($P = 0.003$) depleted, respectively, in ALS CSF samples. Similarly, miR-3168 and miR-625-3p were 69% ($P = 0.1$) and 61% ($P = 0.01$) depleted, respectively, following AGO2 immunoprecipitation in healthy control CSF samples, but appear to be refractory to depletion ($P = 0.058$) in ALS CSF (Fig. 4*B* and Datasets S4 and S5). These observations suggest that certain miRNAs may be associated with either of the two broad classes of immunologically distinguishable complexes in CSF, depending on the pathophysiological conditions. Under normal physiological conditions, CSF miRNAs appear to be primarily associated with miRISC/AGO2 complexes that are accessible by anti-AGO2 antibodies, while, under certain pathological conditions, CSF miRNA may be associated with complexes that are unable to interact with AGO2 antibodies.

We also conducted AGO2 immunoprecipitation in 400 μL of CSF from patients with elevated intracranial pressure (ICP). AGO2 immunoprecipitation from ICP CSF (Fig. 4*C*) resulted in a pattern of miRNA depletion that was different from normal CSF. Similar to what was observed in ALS CSF, certain miRNAs were resistant to AGO2 immunoprecipitation (average depletion of ~48%; Fig. 4*F*). For example, miR-203b-5p, miR-203a-3p, miR-152-5p, miR-1911-5p, and miR-138-2-3p were each more than 50% depleted ($P \leq 0.05$) in healthy control CSF, while they were completely refractory to depletion ($P \leq 0.05$) in ICP CSF samples. Similarly, miR-9-5p and miR-125a-5p were also more than 50% depleted ($P \leq 0.05$) by AGO2 immunoprecipitation in healthy control CSF but were less than 50% depleted ($P \leq 0.05$) in the ICP CSF samples (Datasets S6 and S7).

Discussion

We observed that almost all of the miRNAs in normal human plasma could be immunoprecipitated by AGO2 antibodies, suggesting that the majority of plasma-borne miRNAs are associated with miRISC/AGO2 complexes that are free to interact with anti-AGO2 antibodies (Fig. 1). Across 5 independent samples of plasma small RNA sequencing, only 11 miRNAs were less than 50% depleted by AGO2 immunoprecipitation; apparently, a substantial fraction of these 11 miRNAs (miR-155, miR141-3p, miR-375, miR-223-3p, miR-10b, miR-125a-5p, miR-125b-5p, miR-29b-3p, miR-30e-3p, miR-30a-5p, and miR-126-3p) are associated with complexes in which AGO2 is absent or inaccessible to anti-AGO2 antibodies (Fig. 1). It is possible that the antibody-inaccessible fraction of these 11 miRNAs reflects enclosure within EVs, as these same miRNAs have been previously reported to be exosome-associated (15, 35–39). It should be noted that, in our experiments, some portion of the miRNAs that were not immunoprecipitated with AGO2 could be associated with AGO1, AGO3, or AGO4; we did not assess the contribution of these other Argonautes to circulating miRISC, as our antibody was specific to AGO2.

In support of the conclusion that miRNAs in circulation are predominantly miRISC-associated, we find that the two miRNAs that we tested (let-7 and miR-16) can base-pair with a complementary 2′-O-methyl oligonucleotide target mimic in a sequence-specific manner. Moreover, the binding of circulating miRNAs to a target mimic appears to be mediated by seed nucleotide (nucleotides g2 to g8) base pairing. In particular, we observed that miR-16 family members with identical seed sequences but divergent nonseed (nucleotides g9 to g22) sequences were depleted from plasma using a target oligo complementary to miR-16. Further, miR-107/miR-103 family members, which fortuitously match a portion of the miR-16 target through their seed sequence, also are efficiently depleted from plasma along with miR-16. The ability of circulating miRNAs to engage in seed-mediated base

pairing to a target mimic oligonucleotide is consistent with bona fide miRISC-mediated target recognition (40–44). Also consistent with the association of circulating miRNAs with active miRISC, we find that the amount of AGO2 recovered from plasma by a target mimic oligo is similar to the amount of the cognate miRNA in the plasma sample, suggesting a 1:1 ratio between a circulating miRNA and its AGO2 partner.

In contrast to the miR-16 family members detected, which were efficiently depleted from plasma by a miR-16 complementary 2′-O-methyl target mimic oligonucleotide, let-7 family members were less efficiently depleted by a cognate let-7a target mimic. One interpretation of this observation is that a portion of some circulating miRNAs (exemplified by the let-7 family) may be sequestered within vesicles or in higher-order protein complexes that mask the miRNA in such a way that inhibits the base pairing with a target mimic. An alternative explanation for inefficient depletion of a miRNA from plasma using target mimics could be the presence of an endogenous cRNA including unreleased passenger strand already annealed to the miRNA. However, we think that this latter explanation is unlikely for two reasons. First, we did not observe appreciable representation of passenger strand read counts relative to guide strand reads in our datasets (*SI Appendix*, Tables S3–S5). In particular, the let-7 family member with the highest fraction of passenger strand detected in plasma was let-7d (4.83% of the two strands), while it was 61% depleted by 2′-OM pull-down (*SI Appendix*, Table S5). Second, our RNA sequencing data of plasma supernatant from control experiments (*SI Appendix*, Table S6) and of plasma RNA immunoprecipitated by anti-AGO2 antibody (*SI Appendix*, Table S7) did not indicate an appreciable representation of mappable RNA species other than miRNA.

We observed that the miRNA profile in plasma was not quantitatively affected by freeze-thawing the sample, nor by the incubation times and conditions of our immunoprecipitation and target mimic experimental conditions. Other researchers have also observed that the levels of miRNAs associated with exosomes is not affected in frozen plasma compared with fresh plasma, suggesting that EVs are stable during freeze-thawing (7). The association of circulating miRNAs with miRISC/AGO2 complexes could in part account for the remarkable stability of miRNA in body fluids (5, 6), as miRNA bound to AGO2 is held in a conformation where the phosphodiester backbone appears to be protected from nucleases by interactions with AGO2 (45). Moreover, AGO2 loaded with a miRNA appears to adopt a conformation that is resistant to proteases, such as thermolysin (46).

Our findings that plasma-borne miRNAs are associated with miRISC and can sequence-specifically bind to complementary target oligonucleotides implies that these extracellular miRNAs could, in principle, contribute to cellular posttranscriptional gene regulation, provided that they were reinternalized into cells in sufficient quantities. However, it is important to consider that the intracellular concentrations of a miRNA required for efficient gene regulation is estimated to be appreciably greater than ∼20 pM, the K_d for miRISC::target binding (34, 47), and perhaps even in the nanomolar range (4). Our data confirm previous estimates by others (48–50) that the total concentration of circulating miRNAs in blood plasma is approximately ∼5 pM. In our plasma samples, the most abundant miRNAs, miR-451 and miR-16, are present in concentrations of ∼2.5 pM and 0.5 pM, respectively, indicating that even these relatively abundant circulating miRNAs would need to be concentrated 10 to 1,000 fold upon import into the cytoplasm of recipient cells in order to be functional. Further in vivo studies are necessary to determine whether certain circumstances could make it possible for cells to import miRNAs at functional levels from the extracellular milieu.

By analogy with synthetic miRNAs and siRNAs, whose in vivo delivery to cells are facilitated by the interactions of their ligand conjugates and the cell surface receptors (51, 52), uptake of natural extracellular miRISC could be mediated by cell surface proteins with the capacity to bind AGO2. Neuropilin-1 is one such cell surface protein suggested to bind AGO2 (53). It is also likely that the fate of some extracellular miRNAs could be determined by association (either internally or externally) with EVs (Fig. 1). Although we observed that the majority of plasma miRNAs are associated with free miRISC, based on their ability to readily interact with anti-AGO2 antibody and target mimics, we did not assess what fraction of circulating miRISC in our samples could be bound to the exterior surfaces of EVs. Support for the association of miRISC with EVs comes from various reports, including the identification of AGO2 and GW182 in exosomal samples recovered from cell culture medium (25). However, previous studies that have reported EV-associated miRNAs have generally not included confirmation of whether the reported miRNAs/miRISC/AGO2 are enclosed within the EV interior or, alternatively, bound to the exterior surface of EVs.

Circulating miRNAs have been investigated as potential diagnostic markers for numerous diseases, including cancer (11, 12), liver toxicity (14), and neurodegenerative disorders (10, 13). What has not been explored is the question of possible disease-related differences in the assortment of circulating miRNAs into distinct carrier complexes, such as free miRISC/AGO2 and EVs. It is not yet understood whether the assortment of extracellular miRNAs into particular complexes may reflect the cell type and/or pathophysiological status of their cells of origin. Numerous reports suggest that cells may produce elevated levels of EVs under pathological conditions, such as in the tumor microenvironment (54, 55). EV-associated miRNAs have been reported to be released through a ceramide-dependent secretion pathway (31), and accumulation of ceramide has been reported in spinal cords of ALS patients (56) and in brain cortices of Alzheimer's disease patients (9).

We observed that extracellular miRNAs in CSF samples from healthy individuals were predominantly depleted by AGO2 immunoprecipitation, while CSF from ALS patients contained a subset of miRNAs that were inefficiently depleted by AGO2 immunoprecipitation. Similarly, CSF from patients with elevated intracranial pressure contained a higher portion, compared to normal CSF, of miRNAs that were not efficiently depleted by AGO2 immunoprecipitation. These observations suggest that pathological conditions may alter not only the overall profile of miRNA levels in CSF (57–59), but also the profile of miRNA carrier complexes. Further investigations will be required to characterize the origin and composition of anti-AGO2–refractory miRNA complexes in CSF and to determine their potential significance as a novel class of diagnostic biomarkers in the context of neurological diseases. More broadly, we suggest that employing methods to resolve circulating miRNAs profiles into classes of carrier complexes such as those reported here—free miRISC complexes that are compliant with AGO2 immunoprecipitation and/or that can base-pair with a target mimic, and complexes that are refractory to these biochemical assays—could substantially increase the specificity of biomarker discovery for diverse pathological conditions. To this end, it will be important to further characterize in detail the properties and molecular compositions of extracellular miRNA complexes, both in normal and pathological contexts, and to uncover the cellular processes and export pathways that produce them.

Materials and Methods

Detailed materials and methods used in all experiments are provided in *SI Appendix, SI Methods*. AGO2 immunoprecipitation was conducted according

to Arroyo et al. (6), and 2′-O-methyl RNA oligonucleotide target mimic pull-down assay was conducted according to Jannot et al. (60). Plasma and CSF RNA was extracted according to Tanriverdi et al. (61), and qRT-PCR was conducted according to Geekiyanage et al. (9). Small-RNA libraries were prepared using QIAseq miRNA Library Kit (Qiagen), and RNA sequencing was conducted using Illumina platforms. Small-RNA sequencing data analysis was conducted using the Qiagen pipeline, Deseq2 (62), Student *t* tests, and debrowser platforms (63).

Human Plasma and CSF Sample Collection. Deidentified human plasma and CSF samples were collected in accordance with procedures and consent forms approved by the University of Massachusetts Medical School Institutional Review Board (IRB 13019_12 and IRB 14047_12). Deidentified healthy control and ALS CSF samples were obtained from the NEALS consortium (https://www.neals.org/).

Data Availability. All study data are included in the article and *SI Appendix*.

ACKNOWLEDGMENTS. This research was supported by the Angel Fund and NIH Grants R01GM088365 and R01GM034028. The mass spectrometry analysis was supported by NIH Grant GM089778. We thank Phillip Zamore, PhD, for providing the human AGO2 standards. We thank Carolina Ionete, MD, for providing the ICP CSF samples and the Northeast ALS Consortium (NEALS) for providing the healthy control and ALS CSF samples.

1. L. He, G. J. Hannon, MicroRNAs: Small RNAs with a big role in gene regulation. *Nat. Rev. Genet.* **5**, 522–531 (2004).
2. V. Ambros, MicroRNA pathways in flies and worms: Growth, death, fat, stress, and timing. *Cell* **113**, 673–676 (2003).
3. D. P. Bartel, MicroRNAs: Genomics, biogenesis, mechanism, and function. *Cell* **116**, 281–297 (2004).
4. A. D. Bosson, J. R. Zamudio, P. A. Sharp, Endogenous miRNA and target concentrations determine susceptibility to potential ceRNA competition. *Mol. Cell* **56**, 347–359 (2014).
5. A. Turchinovich, L. Weiz, A. Langheinz, B. Burwinkel, Characterization of extracellular circulating microRNA. *Nucleic Acids Res.* **39**, 7223–7233 (2011).
6. J. D. Arroyo *et al*., Argonaute2 complexes carry a population of circulating microRNAs independent of vesicles in human plasma. *Proc. Natl. Acad. Sci. U.S.A.* **108**, 5003–5008 (2011).
7. J. R. Chevillet *et al*., Quantitative and stoichiometric analysis of the microRNA content of exosomes. *Proc. Natl. Acad. Sci. U.S.A.* **111**, 14888–14893 (2014).
8. R. Raoof *et al*., Cerebrospinal fluid microRNAs are potential biomarkers of temporal lobe epilepsy and status epilepticus. *Sci. Rep.* **7**, 3328 (2017).
9. H. Geekiyanage, C. Chan, MicroRNA-137/181c regulates serine palmitoyltransferase and in turn amyloid β, novel targets in sporadic Alzheimer's disease. *J. Neurosci.* **31**, 14820–14830 (2011).
10. H. Geekiyanage, G. A. Jicha, P. T. Nelson, C. Chan, Blood serum miRNA: Non-invasive biomarkers for Alzheimer's disease. *Exp. Neurol.* **235**, 491–496 (2012).
11. Z. Huang *et al*., A novel serum microRNA signature to screen esophageal squamous cell carcinoma. *Cancer Med.* **6**, 109–119 (2017).
12. F. Li, J. Huang, J. Liu, W. Xu, Z. Yuan, Multivariate analysis of clinicopathological and prognostic significance of miRNA 106b~25 cluster in gastric cancer. *Cancer Cell Int.* **19**, 200 (2019).
13. C. Ricci, C. Marzocchi, S. Battistini, MicroRNAs as biomarkers in amyotrophic lateral sclerosis. *Cells* **7**, 219 (2018).
14. J. Ward *et al*., Circulating microRNA profiles in human patients with acetaminophen hepatotoxicity or ischemic hepatitis. *Proc. Natl. Acad. Sci. U.S.A.* **111**, 12169–12174 (2014).
15. W. Ying *et al*., Adipose tissue macrophage-derived exosomal miRNAs can modulate in vivo and in vitro insulin sensitivity. *Cell* **171**, 372–384.e12 (2017).
16. K. C. Vickers, B. T. Palmisano, B. M. Shoucri, R. D. Shamburek, A. T. Remaley, MicroRNAs are transported in plasma and delivered to recipient cells by high-density lipoproteins. *Nat. Cell Biol.* **13**, 423–433 (2011).
17. Y. T. Tang *et al*., Comparison of isolation methods of exosomes and exosomal RNA from cell culture medium and serum. *Int. J. Mol. Med.* **40**, 834–844 (2017).
18. L. Zhao *et al*., Isolation and Identification of miRNAs in exosomes derived from serum of colon cancer patients. *J. Cancer* **8**, 1145–1152 (2017).
19. E. N. Prendergast *et al*., Optimizing exosomal RNA isolation for RNA-Seq analyses of archival sera specimens. *PLoS One* **13**, e0196913 (2018).
20. K. Wang, S. Zhang, J. Weber, D. Baxter, D. J. Galas, Export of microRNAs and microRNA-protective protein by mammalian cells. *Nucleic Acids Res.* **38**, 7248–7259 (2010).
21. X. Chen *et al*., Characterization of microRNAs in serum: A novel class of biomarkers for diagnosis of cancer and other diseases. *Cell Res.* **18**, 997–1006 (2008).
22. P. S. Mitchell *et al*., Circulating microRNAs as stable blood-based markers for cancer detection. *Proc. Natl. Acad. Sci. U.S.A.* **105**, 10513–10518 (2008).
23. Y. Zhang *et al*., Secreted monocytic miR-150 enhances targeted endothelial cell migration. *Mol. Cell* **39**, 133–144 (2010).
24. A. Zernecke *et al*., Delivery of microRNA-126 by apoptotic bodies induces CXCL12-dependent vascular protection. *Sci. Signal.* **2**, ra81 (2009).
25. D. J. Gibbings, C. Ciaudo, M. Erhardt, O. Voinnet, Multivesicular bodies associate with components of miRNA effector complexes and modulate miRNA activity. *Nat. Cell Biol.* **11**, 1143–1149 (2009).
26. A. J. McKenzie *et al*., KRAS-MEK signaling controls Ago2 sorting into exosomes. *Cell Rep.* **15**, 978–987 (2016).
27. S. R. Horman *et al*., Akt-mediated phosphorylation of argonaute 2 downregulates cleavage and upregulates translational repression of microRNA targets. *Mol. Cell* **50**, 356–367 (2013).
28. K. Ohshima *et al*., Let-7 microRNA family is selectively secreted into the extracellular environment via exosomes in a metastatic gastric cancer cell line. *PLoS One* **5**, e13247 (2010).
29. T. Thomou *et al*., Adipose-derived circulating miRNAs regulate gene expression in other tissues. *Nature* **542**, 450–455 (2017).
30. H. Valadi *et al*., Exosome-mediated transfer of mRNAs and microRNAs is a novel mechanism of genetic exchange between cells. *Nat. Cell Biol.* **9**, 654–659 (2007).
31. M. Mittelbrunn *et al*., Unidirectional transfer of microRNA-loaded exosomes from T cells to antigen-presenting cells. *Nat. Commun.* **2**, 282 (2011).
32. J. Skog *et al*., Glioblastoma microvesicles transport RNA and proteins that promote tumour growth and provide diagnostic biomarkers. *Nat. Cell Biol.* **10**, 1470–1476 (2008).
33. K. E. A. Max *et al*., Human plasma and serum extracellular small RNA reference profiles and their clinical utility. *Proc. Natl. Acad. Sci. U.S.A.* **115**, E5334–E5343 (2018).
34. L. M. Wee, C. F. Flores-Jasso, W. E. Salomon, P. D. Zamore, Argonaute divides its RNA guide into domains with distinct functions and RNA-binding properties. *Cell* **151**, 1055–1067 (2012).
35. S. Meltzer *et al*., Circulating exosomal miR-141-3p and miR-375 in metastatic progression of rectal cancer. *Transl. Oncol.* **12**, 1038–1044 (2019).
36. S. Wang *et al*., Differentially expressed miRNAs in circulating exosomes between atrial fibrillation and sinus rhythm. *J. Thorac. Dis.* **11**, 4337–4348 (2019).
37. R. Singh, R. Pochampally, K. Watabe, Z. Lu, Y. Y. Mo, Exosome-mediated transfer of miR-10b promotes cell invasion in breast cancer. *Mol. Cancer* **13**, 256 (2014).
38. R. Teruel-Montoya *et al*., Differential miRNA expression profile and proteome in plasma exosomes from patients with paroxysmal nocturnal hemoglobinuria. *Sci. Rep.* **9**, 3611 (2019).
39. X. Jin *et al*., Evaluation of tumor-derived exosomal miRNA as potential diagnostic biomarkers for early-stage non-small cell lung cancer using next-generation sequencing. *Clin. Cancer Res.* **23**, 5311–5319 (2017).
40. S. A. Gorski, J. Vogel, J. A. Doudna, RNA-based recognition and targeting: Sowing the seeds of specificity. *Nat. Rev. Mol. Cell Biol.* **18**, 215–228 (2017).
41. N. T. Schirle, J. Sheu-Gruttadauria, I. J. MacRae, Structural basis for microRNA targeting. *Science* **346**, 608–613 (2014).
42. W. E. Salomon, S. M. Jolly, M. J. Moore, P. D. Zamore, V. Serebrov, Single-molecule imaging reveals that argonaute reshapes the binding properties of its nucleic acid guides. *Cell* **162**, 84–95 (2015).
43. S. D. Chandradoss, N. T. Schirle, M. Szczepaniak, I. J. MacRae, C. Joo, A dynamic search process underlies microRNA targeting. *Cell* **162**, 96–107 (2015).
44. M. H. Jo *et al*., Human argonaute 2 has diverse reaction pathways on target RNAs. *Mol. Cell* **59**, 117–124 (2015).
45. N. T. Schirle, I. J. MacRae, The crystal structure of human argonaute2. *Science* **336**, 1037–1040 (2012).
46. E. Elkayam *et al*., The structure of human argonaute-2 in complex with miR-20a. *Cell* **150**, 100–110 (2012).
47. J. A. Broderick, P. D. Zamore, Competitive endogenous RNAs cannot alter microRNA function in vivo. *Mol. Cell* **54**, 711–713 (2014).
48. C. H. Sterling, I. Veksler-Lublinsky, V. Ambros, An efficient and sensitive method for preparing cDNA libraries from scarce biological samples. *Nucleic Acids Res.* **43**, e1 (2015).
49. Z. Williams *et al*., Comprehensive profiling of circulating microRNA via small RNA sequencing of cDNA libraries reveals biomarker potential and limitations. *Proc. Natl. Acad. Sci. U.S.A.* **110**, 4255–4260 (2013).
50. A. Turchinovich, A. G. Tonevitsky, B. Burwinkel, Extracellular miRNA: A collision of two paradigms. *Trends Biochem. Sci.* **41**, 883–892 (2016).
51. E. Song *et al*., Antibody mediated in vivo delivery of small interfering RNAs via cell-surface receptors. *Nat. Biotechnol.* **23**, 709–717 (2005).
52. R. M. Schiffelers *et al*., Cancer siRNA therapy by tumor selective delivery with ligand-targeted sterically stabilized nanoparticle. *Nucleic Acids Res.* **32**, e149 (2004).
53. G. J. Prud'homme, Y. Glinka, Z. Lichner, G. M. Yousef, Neuropilin-1 is a receptor for extracellular miRNA and AGO2/miRNA complexes and mediates the internalization of miRNAs that modulate cell function. *Oncotarget* **7**, 68057–68071 (2016).

54. A. Mantovani, P. Allavena, A. Sica, F. Balkwill, Cancer-related inflammation. *Nature* **454**, 436–444 (2008).
55. K. Al-Nedawi *et al*., Intercellular transfer of the oncogenic receptor EGFRvIII by microvesicles derived from tumour cells. *Nat. Cell Biol.* **10**, 619–624 (2008).
56. R. G. Cutler, W. A. Pedersen, S. Camandola, J. D. Rothstein, M. P. Mattson, Evidence that accumulation of ceramides and cholesterol esters mediates oxidative stress-induced death of motor neurons in amyotrophic lateral sclerosis. *Ann. Neurol.* **52**, 448–457 (2002).
57. R. Waller *et al*., Small RNA sequencing of sporadic amyotrophic lateral sclerosis cerebrospinal fluid reveals differentially expressed miRNAs related to neural and glial activity. *Front. Neurosci.* **11**, 731 (2018).
58. M. Benigni *et al*., Identification of miRNAs as potential biomarkers in cerebrospinal fluid from amyotrophic lateral sclerosis patients. *Neuromolecular Med.* **18**, 551–560 (2016).
59. A. Freischmidt, K. Müller, A. C. Ludolph, J. H. Weishaupt, Systemic dysregulation of TDP-43 binding microRNAs in amyotrophic lateral sclerosis. *Acta Neuropathol. Commun.* **1**, 42 (2013).
60. G. Jannot, A. Vasquez-Rifo, M. J. Simard, Argonaute pull-down and RISC analysis using 2′-O-methylated oligonucleotides affinity matrices. *Methods Mol. Biol.* **725**, 233–249 (2011).
61. K. Tanriverdi *et al*., Comparison of RNA isolation and associated methods for extracellular RNA detection by high-throughput quantitative polymerase chain reaction. *Anal. Biochem.* **501**, 66–74 (2016).
62. M. I. Love, W. Huber, S. Anders, Moderated estimation of fold change and dispersion for RNA-seq data with DESeq2. *Genome Biol.* **15**, 550 (2014).
63. A. Kucukural, O. Yukselen, D. M. Ozata, M. J. Moore, M. Garber, DEBrowser: Interactive differential expression analysis and visualization tool for count data. *BMC Genom.* **20**, 6 (2019).